Article:
Cao, H, Amador, C, Jia, X orcid.org/0000-0001-8590-7477 et al. (2 more authors) (2016) A modelling framework for bulk particles dissolving in turbulent regime. Chemical Engineering Research and Design, 114. pp. 108-118. ISSN 0263-8762

https://doi.org/10.1016/j.cherd.2016.08.012

A Modelling Framework for Bulk Particles Dissolving in Turbulent Regime

Hui Cao[1,], Carlos Amador[2], Xiaodong Jia[3], Yongliang Li[1] and Yulong Ding[1]*

[1]School of Chemical Engineering, University of Birmingham, B15 2TT, United Kingdom

[2] Proctor & Gamble Newcastle Innovation Centre, Newcastle Upon Tyne, NE12 9TS, United Kingdom

[3]School of Chemical and Process Engineering, University of Leeds, LS2 9JT, United Kingdom

Corresponding Author *h.cao@bham.ac.uk

ABSTRACT A mixing-tank model combining CFD simulation and Noyes-Whitney equation has been demonstrated for predicting dissolution of spray-dried detergent powder. The dissolution behaviour of bulk particles has been directly linked to the input power of the mixing system which is highly desired by industry with the aim of reducing testing when extrapolating particle dissolution performance from bench scale measurements to any washing system/condition. Initial particle parameters such as density, solubility, size distribution and diffusivity were considered. The model was first validated with experiment of non-porous single-ingredient particle Na_2CO_3 granules. Later, porous multi-ingredients particles from spray-drying pilot were

used to validate the model with dissolution experiment data. The good agreements between experiment and simulation at different agitating speeds and temperatures illustrated that the model can be used for predicting bulk particles dissolving in a turbulent regime where they are well suspended in the mixing system. The CFD simulation results revealed detail information about energy dissipation rate across the vessel which explained the phenomena that when non-porous Na_2CO_3 granules were not well mixed in the system, dissolution predicted by modelling was much faster than experiment, indicating that local energy dissipation rate could be one solution to improve the modelling accuracy of this case.

KEYWORDS Dissolution, Simulation, Detergent powder, Turbulent regime

1. INTRODUCTION

Growing needs exist for a separate means of assessing dissolving performance via the formulation development process in a variety of applications such as pharmaceutics, food, and detergent. Since a large number of compounds may be involved, a model, which is capable of predicting porous particle dissolving in different mixing system, is particularly desirable to minimize the amount of experimental work. Once such a model is established, two strategies can be applied. First, a number of new chemical compounds with desirable activity can be compared for transport properties, which leads to the selection of right candidate with the most desirable combination of properties (Dressman and Fleisher, 1986). Second, formulation and administration time can be fine-tuned to optimize product design by simulating dissolving performance under the various conditions (Dressman and Fleisher, 1986). This second strategy can be very helpful for detergent powder industries. Reducing testing when extrapolating particle

dissolution performance from bench scale measurements to any washing system/condition (front loading, top loading, hand washing etc.) could significantly shorter product designing process.

The detergent powder contains mainly sodium sulphate, sodium carbonate, linear alkylbenzene sulphonate (LAS), sodium silicate, polymer etc (Van Dalen et al., 2011). Spray-dried detergent powder can be considered as hollow primary particles agglomerate together, and they dissolves instantly when added to water (Davidsohn, 1978). Forny et al. summarized the dissolution process of these powder as i) the wetting of the powder where water penetrates into the pore system due to capillary forces; ii) the immersion of powder into water; iii) the dissolution of the solid bridges between primary particles followed by powder disintegration; and iv) the dissolution of soluble primary particles (Forny et al., 2011; Schubert, 1987). These steps might happen simultaneously rather than sequentially depending on physical and chemical properties of powder (e.g., particle size, density, porosity, and chemical composition) and dissolving liquid (e.g., liquid surface tension, viscosity, density, temperature, and diffusion/convection). Developing a model with all the four steps to simulate the dissolution of such complex particles is rather ambitious than realistic. Effort has been put into more practical strategy to simulate these steps separately. It is evident that a variety of dissolution models have been developed from different applications such as pharmaceutics (Jia and Williams, 2007), petroleum (Kang et al., 2002), metallurgy (Arnout et al., 2008), geology (Pereira Nunes et al., 2016) and food (Yuan et al., 2013). In most of the studies, the models focus on single particle or a small cluster. With the assistance of sophisticated experiment approach for characterising particle structures such as X-ray microtomography (Ansari and Stepanek, 2007; Ansari and Stepanek, 2008; Jia and Williams, 2007; Pereira Nunes et al., 2016), particle dissolution process such as UV-Vis spectroscopy and static light scattering (Smrčka et al.), these models can reveal detail information for example

pore and particle structure (Ansari and Stepanek, 2008; Yuan et al., 2013), flow rate distribution within pores (Pereira Nunes et al., 2016), particle porosity (Ansari and Stepanek, 2008), primary particle size and spatial location within particle (Ansari and Stepanek, 2008). However, scaling up of these models to simulate bulk particles dissolving in severe flow conditions (washing machine) can be extremely time consuming and also require powerful computers.

With the strong desire from detergent industry aiming at reducing testing when extrapolating particle dissolution performance from bench scale measurements to any washing system/condition, a framework has been developed to simulate spray-dried detergent powder dissolving in a mixing-tank. The model combines CFD simulation and Noyes-Whitney equation (Noyes and Whitney, 1897) with initial particle parameters such as density, solubility, size distribution, and diffusivity. The power input of the dissolution system is linked with particle mass transfer rate by the Sherwood number which is obtained through energy dissipation rate in the system. The framework is first validated with dissolution experiment of non-porous single-ingredient particle Na_2CO_3 granule. Later, multi-ingredients porous particles from spray-drying pilot are used to validate model which further proves that the model can be used for predicting bulk particles dissolving under turbulent regime where they are well suspended in the dissolution system.

2. MODEL DESCRIPTION

2.1 Equation derivation

When external mass transfer limitation at the particle surface boundary layer controls the particle dissolution rate, it can be modelled by Noyes-Whitney equation:

$$\frac{dM_t}{dt} = -K \cdot A_t \cdot (C_s - C_t) \quad (1)$$

where M_t is the remaining mass of particles at time t, K is the mass transfer coefficient, A_t is the exposing surface area of particle to solvent at time t, C_s is the solubility of the material (saturated concentration) and C_t is solution concentration at time t (Noyes and Whitney, 1897). In most washing system, $C \ll C_s$.

In convective dissolution condition, the dimensionless number Sherwood number (Sh) is introduced to represent the ratio of convective to diffusive mass transport:

$$Sh = \frac{K \cdot L}{D} \quad (2)$$

where L is the characteristic length and D is diffusivity. Then mass transfer coefficient for a spherical particle can be written as:

$$K = \frac{Sh \cdot D}{d_{p,t}} \quad (3)$$

where $d_{p,t}$ is the particle diameter at dissolution time t.

Assuming particles are homogeneous, and then the particle density ρ_p is constant throughout dissolution. Given a number of $N_{particle}$ mono-sized particles, the total initial mass of particles M_0 is:

$$M_0 = N_{particle} \cdot \rho_p \cdot \frac{1}{6} \cdot \pi \cdot d_{p,0}^{\ 3} \quad (4)$$

where $d_{p,0}$ is the initial particle diameter. The total particle number $N_{particle}$ can be expressed as:

$$N_{particle} = \frac{6 \cdot M_0}{\rho_p \cdot \pi \cdot d_{p,0}^{\ 3}} \tag{5}$$

So the remaining mass of particles M_t at time t can be expressed as:

$$M_t = N_{particle} \cdot \rho_p \cdot \frac{1}{6}\pi \cdot d_{p,t}^3 = \left(\frac{6 \cdot M_0}{\pi \cdot \rho_p \cdot d_{p,0}^3} \right) \cdot \rho_p \cdot \frac{1}{6} \cdot \pi \cdot d_{p,t}^3 = M_0 \cdot \left(\frac{d_{p,t}}{d_{p,0}} \right)^3 \tag{6}$$

Hence $d_{p,t} = d_{p,0} \cdot \left(\frac{M_t}{M_0} \right)^{1/3}$ (7)

Similarly, the total surface area of the particles exposing to solvent at time t can be given by

$$A_t = N_{particle} \cdot \pi \cdot d_{p,t}^2 = N_{particle} \cdot \pi \cdot d_{p,0}^2 \left(\frac{M_t}{M_0} \right)^{2/3} = A_0 \cdot \left(\frac{M_t}{M_0} \right)^{2/3} \tag{8}$$

where A_0 is the initial surface area of particles.

Substituting Equation (1) with Equation (3) and (8), and assuming $C \ll C_s$, Sherwood number can be introduced to the Noyes-Whitney equation which gives:

$$\frac{dM_t}{dt} = -\frac{Sh \cdot D}{d_{p,t}} \cdot A_t \cdot C_s = -\frac{Sh \cdot D}{d_{p,0}} \cdot A_0 \cdot C_s \cdot \left(\frac{M}{M_0} \right)^{1/3} \tag{9}$$

Many different expressions have been developed to calculate the Sherwood number for a spherical particle that works well under different assumptions. When particles are well mixed inside a stirring tank, the following expression can be used (Koganti et al., 2010)

$$Sh = 2 + 0.47 \cdot \left(\frac{\rho_f \cdot \varepsilon^{1/3} \cdot d_{p,t}^{4/3}}{\mu_f}\right)^{0.62} \cdot \left(\frac{\mu_f}{\rho_f \cdot D}\right)^{0.36} \cdot \left(\frac{d_{impeller}}{d_{tank}}\right)^{0.17} \quad (10)$$

where ρ_f is the solvent density, ε is the turbulent energy dissipation rate, μ_f is the solvent viscosity, $d_{impeller}$ is the diameter of impeller, and d_{tank} is the diameter of the stirring tank. Equation (10) requires particle size changing information during dissolution. Under turbulent flow condition, a good first approximation is to assume that all the input power dissipates into turbulent energy dissipation rate, thus the average turbulent dissipation rate can be estimated by

$$\varepsilon = \frac{P}{V_f \cdot \rho_f} \quad (11)$$

where P is the input power, and V_f is the volume of the solvent.

The input power P can be calculated by the standard equation from mixing industry which shows the relationship between system power and impeller dimension (Hemrajani and Tatterson, 2004):

$$P = N_P \rho_f N^3 d_{impeller}^5 \quad (12)$$

where N_P is the impeller power number and N is the rotating speed in rpm. The power number N_P (also known as Newton number) is a commonly used dimensionless number relating the resistance force to the inertia force (Shah, 1991). It can be obtained from the handbook (Hemrajani and Tatterson, 2004) for various standard mixing systems. For the cases of dissolution testing apparatus or washing systems, CFD method can be used to calculate this value. In our case, COMSOL CFD module was used.

As indicating in Equation (10), the Sherwood number is related with dynamic diameter of particles. To simplify the integration, we assume the Sherwood number is constant and is calculated with initial particle size. Equation (9) then can be integrated to:

$$M_t^{2/3} = M_0^{2/3} - \frac{2}{3}\frac{Sh \cdot D}{d_{p,0}} \cdot \frac{A_0 \cdot C_s}{M_0^{1/3}} \cdot t \quad (13)$$

Finally, the mass transfer of bulk particles with a size distribution can be calculated by the sum of Equation (13) at each particle size. In summary, the framework of our model is shown in Figure 1.

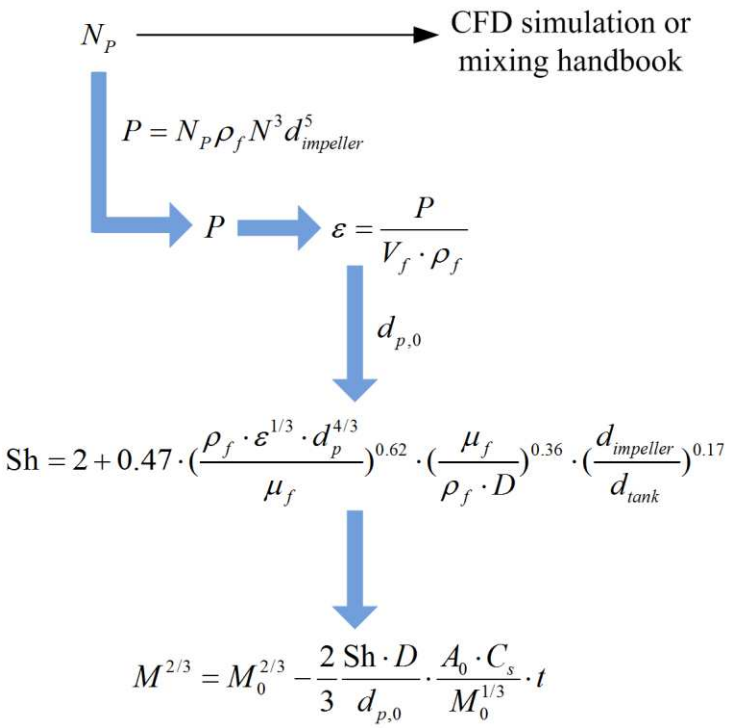

Figure 1. A modelling framework for linking particle dissolution behaviour with mixing system power.

2.2 Simulation in COMSOL

The power number of the dissolution apparatus in the present work was simulated by COMSOL Multiphysics Rotating Machinery, Turbulent Flow Module. A geometry based on dissolution testing apparatus PTWS 610 was built in COMSOL as shown in Figure 2 with 800 mL water. The domain was divided into two parts. The outer tank shape was the fixed part, and the inner cylinder with an impeller surfaces as boundaries was defined as the rotating part. The inner cylinder rotated counter clockwise at a speed of 100, 200 and 300 rpm at 20, 40 and 60 °C respectively. Navier-Stokes equations formulated both in the rotating frame in the inner domain and the fixed coordinated in the outer one. Between outer domain and inner domain, walls were assembled as identity pair. All the other walls were set as non-slip boundary conditions. Water property was applied on the whole domain. Numerical mesh size between 0.02 mm and 0.05 mm was applied.

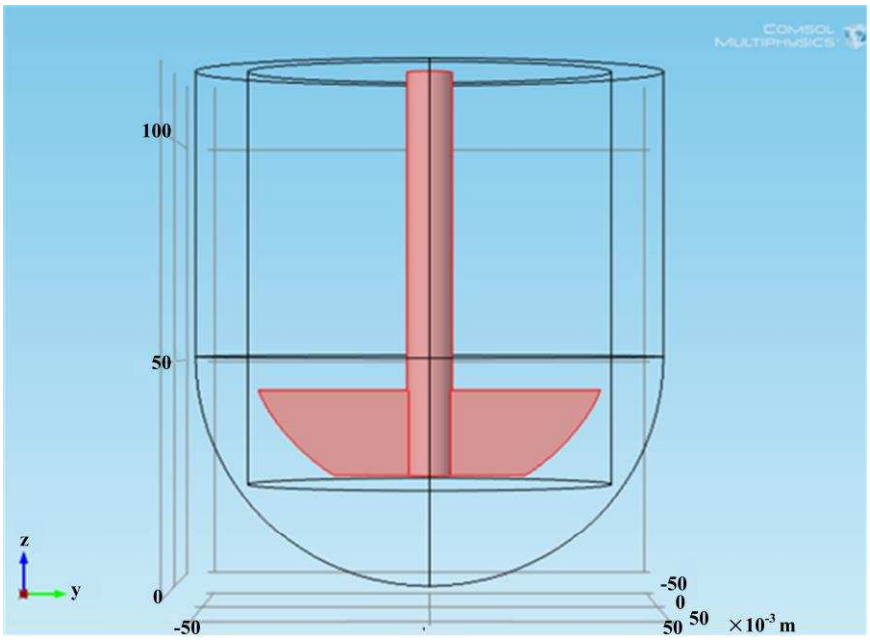

Figure 2. Model geometry of the dissolution testing apparatus PTWS 610 in COMSOL with 800 mL water in the vessel.

The power on the impeller was then calculated by adding the following equation to COMSOL post-process:

$$P = \int_A \Omega \cdot \Gamma dA = \int_A \Omega \cdot (r \times F_{impeller}) dA_{impeller} \quad (14)$$

where $F_{impeller}$ is the force acting on each point of impeller surface, Ω is the rotating speed and can be calculated as $\Omega = 2\pi N$, $A_{impeller}$ is the impeller surface area, Γ is the torque on impeller and $r = \{x, y, z\}$ is the coordinate. Since the impeller shaft is parallel to the z-axis in the model, Equation (14) can be reduced to:

$$P = \int_A 2\pi N(xF_y - yF_x) dA_{impeller} \quad (15)$$

where F_x and F_y are the force components along x- and y-axis. As a result, the impeller power was calculated by integrating the force on the whole impeller surface. Once the impeller power was integrated, the energy dissipation rate was calculated by Equation (11), then the Sherwood number was calculated by Equation (10), and eventually particle dissolution performance was predicted by Equation (13).

3. EXPERIMENT

3.1. Materials

Two types of particles have been used in the present work to validate the model. One is non-porous single-ingredient Na_2CO_3 granule (batch number 1009260NM-019). The other one is porous multi-ingredients powder PANDORA (batch number IPP13-9991-3) manufactured from spray-drying pilot with ingredients such as Na_2CO_3, Na_2SO_4, sodium silicate and LAS. For

PANDORA powders, two size cuts 355-425 µm and 425-600 µm have been used. All the samples were provided by Procter & Gamble Newcastle Innovation Centre.

3.2. Particle characterization

The surface morphology of particles was examined using a portable Hitachi TM3030 PLUS Scanning Electron Microscope (SEM). N_2 adsorption and desorption isotherms were recorded at 77 K on a BET Surface Area analyser (TriStar 3000, Micromeritics). All samples were degassed at 120 °C for 12 h under vacuum before analysis. Particle size distribution (PSD) was measured using laser-diffractometry (GRADIS/L, Sympatec GmbH) with bulk samples dispersed by gravity. The solubility of PANDORA powder were measured by adding small amount of samples into water and measuring solution conductivity with a Conductivity meter (JENWAY 470) until the conductivity stops changing with additional samples. The solubility was measured at 20, 40 and 60 °C. Solubility of Na_2CO_3 granules was consulted from literature (Etacude, 2004-2008).

3.3. Experiment set up of dissolution test

Dissolution test was carried out by adding a population of 0.15 g particles into the dissolution apparatus PTWS 610. The probe of conductivity meter was insert in the apparatus axially parallel to the impeller and located 3 mm above the impeller upper edge and 3 mm to the vessel wall. Each sample was tested at three temperatures 20, 40 and 60 °C with a rotating speed of 100, 200 and 300 rpm respectively. Solution conductivity changes as a function of time was recorded and normalized to obtain particle release profile.

4. RESULTS AND DISCUSSION

4.1. Particle characterization

Figure 3 are SEM images of Na_2CO_3 granules and PANDORA powders in different magnifications. Figure 3 (a) and (b) are Na_2CO_3 at 100 and 1500 times. Particles have rough surfaces with pebble looking small granules on the surface. Figure 3 (c) (d) (e) and (f) are PANDORA powders at 355-425 and 425-600 µm size cuts with 100 and 1500 times magnification, respectively. Different from Na_2CO_3 granules, PANDORA powder has irregular shaped structures with pores on the surface. BET results confirm the existence of pores on particles with more quantitive information for example particle specific surface area, porosity and absolute density (shown in Table 1). Na_2CO_3 granules has no porosity while PANDORA powder has a porosity of 0.41. Specific surface area is slightly different between PANDORA size cuts, probably due to higher agglomeration in larger size range. However, significantly higher value of PANDORA, comparing to Na_2CO_3 granules, indicates that more surface area of PANDORA particles might directly expose to water during dissolution.

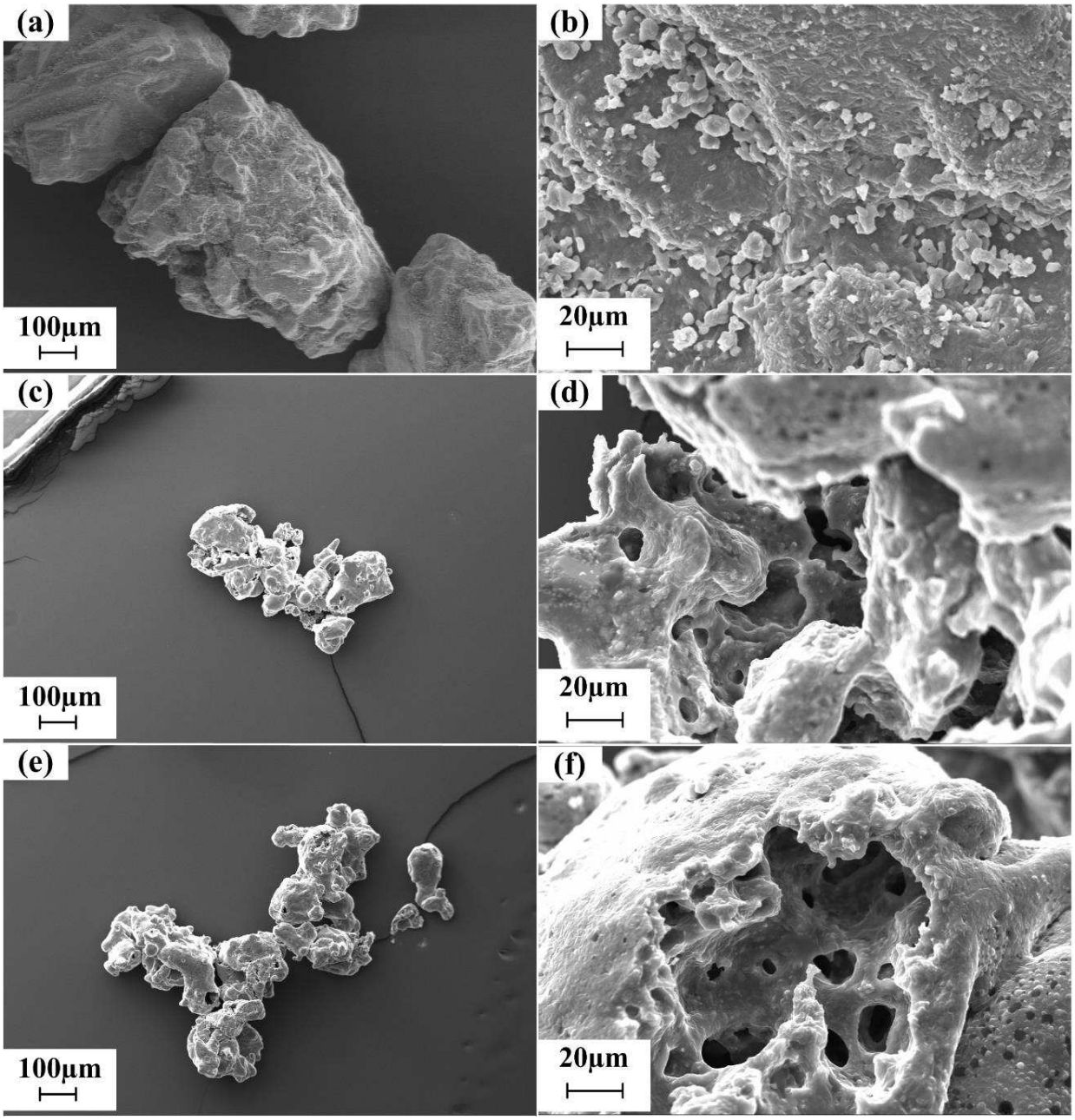

Figure 3. SEM images of particles at 100 and 1500 times magnification (a) (b) Na_2CO_3 granules, (c) (d) PANDORA agglomerates 355-425 µm size cut, and (e) (f) PANDORA agglomerates 425-600 µm size cut.

Table 1. BET results of specific surface area, porosity and absolute density of Na_2CO_3 granules and PANDORA agglomerates. Envelope density is calculated by multiplying absolute density with solid space in particle.

	Na_2CO_3 granule	PANDORA 355-425 µm	PANDORA 425-600 µm
Specific surface area (m^2/g)	0.273	0.332	0.396
Porosity	-	0.41	0.41
Absolute density (kg/m^3)	2540	1914	1914
Envelope density (kg/m^3)	-	1129	1129

Particle size distribution is shown in Figure 4. Apparent differences between the three investigated samples have been detected. Na_2CO_3 granules have the widest size distribution by mass mainly locates between 50 and 1400 µm, while PANDORA particles have much narrower distribution due to the size cut, mainly locating within the size cut range 355-425 µm and 425-600 µm.

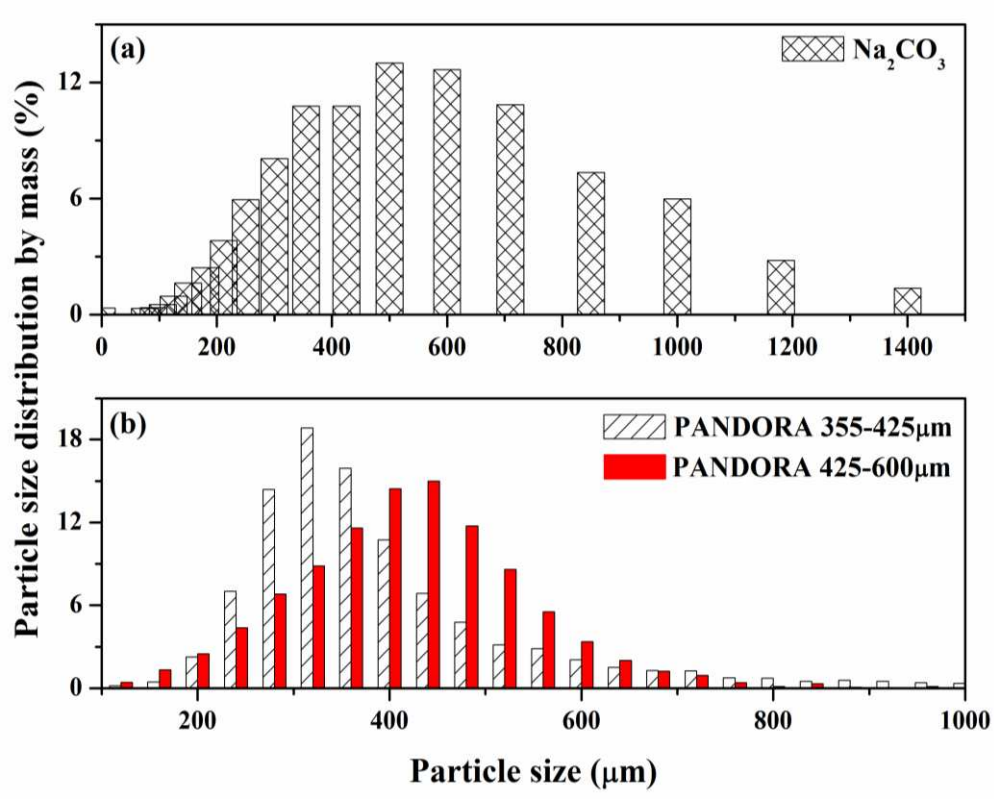

Figure 4. Particle size distribution of (a) Na_2CO_3 granules and (b) PANDORA agglomerates at two different size cuts (355-425 μm and 425-600 μm).

The solubility of Na_2CO_3 granules can be found in literature (Etacude, 2004-2008) which is listed in Table 2. The value increases as solution temperature increasing, and then decreases to a lower value with the highest solubility around 40 °C (Etacude, 2004-2008). The experiment results of the solubility of PANDORA powders are shown in Figure 5. The conductivity of solution increases as dissolved amount of sample increasing, and slowly approaches equilibrium state where conductivity stops changing with additional samples. Comparing to Na_2CO_3, the solubility of PANDORA powders increases as solution temperature increasing. At 40 and 60 °C, PANDORA has lower solubility than Na_2CO_3, but higher at 20 °C.

Table 2. Solubility and diffusivity of Na_2CO_3 granules. Solubility of Na_2CO_3 is from literature (Etacude, 2004-2008). Na_2CO_3 diffusivity is calculated by Nernst equation (Nernst, 1888) at 25 °C and Stokes-Einstein equation (Frenkel, 1946) at 20, 40 and 60 °C.

Temperature (°C)	C_s (kg/m^3) (Etacude, 2004-2008)	D (10^{-9} m^2/s)
20	218.0	1.12
25	-	1.28
40	488.1	1.84
60	464.1	2.74

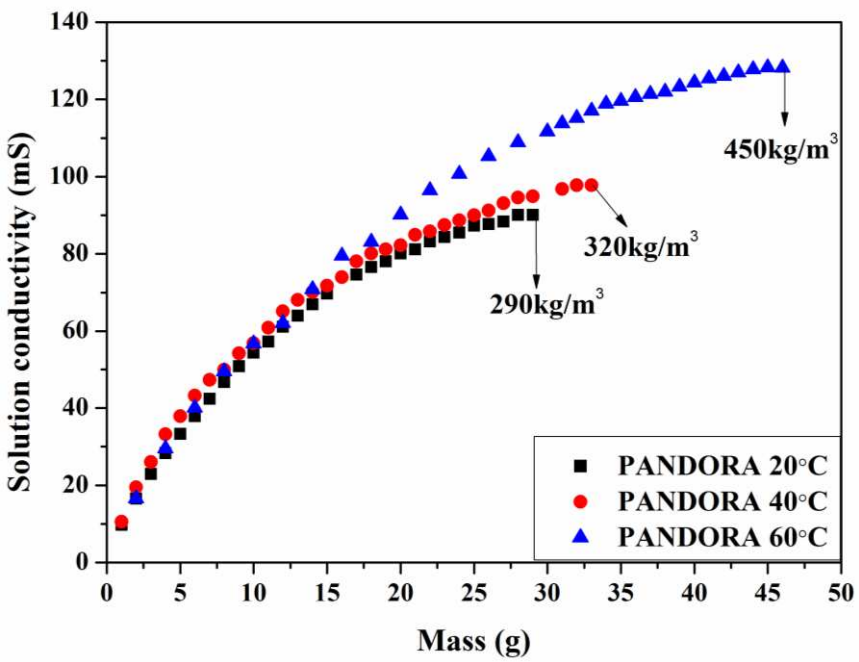

Figure 5. Solubility test of PANDORA 355-425 µm at different temperatures in 100 g de-ionised water.

Diffusivity is one of the key factors for particle dissolution. The diffusivity can be calculated by Nernst equation:

$$D = \frac{RT}{F_c^2}\frac{\lambda_+^\circ \lambda_-^\circ}{\lambda_+^\circ + \lambda_-^\circ}\frac{|Z_-| + |Z_+|}{|Z_+ Z_-|} = 8.931 \times T \frac{\lambda_+^\circ \lambda_-^\circ}{\lambda_+^\circ + \lambda_-^\circ}\frac{|Z_-| + |Z_+|}{|Z_+ Z_-|} \quad (16)$$

in a dilute solution, where R is the ideal gas constant, F_c is the Faraday constant, T is the absolute temperature, λ_+° is the cationic conductance at infinite dilution, λ_-° is the anionic conductance at infinite dilution, Z_+ is the cation valence and Z_- is the anion valence (Nernst, 1888). For Na^+ and CO_3^{2-}, the corresponding λ_+° and λ_-° are 50.1 and 69.3 at 25 °C (Robinson and Stokes, 2012). From the Nernst equation, the diffusivity Na_2CO_3 granules in water at 25 °C is 1.28×10^{-9} m^2/s. As λ_+° and λ_-° values are limited in literature at investigated temperatures, then the diffusivity were calculated by the Stokes-Einstein equation:

$$D = \frac{k_B T}{6\pi r_p \mu_f} \tag{17}$$

where k_B is the Boltzmann's constant, and r_p is the radius of the diffusing particle (cations and anions of the dissolved electrolyte) (Frenkel, 1946). Equation (17) indicates that the diffusivity is proportional to the ratio of T / μ_f. Liquid viscosity μ_f, in the case here (diluted solution), can be considered as water viscosity which can be found from literature. Then, based on the value at 25 °C, the diffusivities of Na_2CO_3 granules calculated by Equation (17) at 20, 40 and 60 °C are shown in Table 2.

4.2. COMSOL simulation results of energy dissipation rate

The impeller inside PTWS 610 dissolution apparatus does not come with power number information. Therefore, COMSOL Multiphysics Rotating Machinary Module was used to calculate the power integrated on the impeller surface. A typical example of power versus time for 20 rpm 20 °C is plotted in Figure 6 (a). The power first increases to the maximum value at 1.7 s, then drops down to a lower value and stablizes after agitating 20 s with some oscillation

inbetween. The power number N_P was calculated by Equation (12) with the stablized power. After several conditions including different rotating speeds and temperatures were simulated, the power number versus the Renolds number is plotted in Figure 6 (b) correspondingly. In the regime where Reynolds number is smaller than 5000, power number varies noticeably. As Reynolds number increases (> 5000), turbulent flow developes further, the power number becomes constant and independent of Reynolds number (Paul et al., 2004) with an average value around 0.882. This power number is between the Marine propeller (N_P 0.35) and the paddle (N_P 2) (Paul et al., 2004), which is reasonable considering the geometry of our impeller is similar to these two and the total surface area is inbetween them, seeing embedded pictures in Figure 6 (b). Turbulent energy dissipation rate is calculated with the result of impeller power number, showing in Table 3. Clearly, the dissipation rate strongly depends on the rotating speed for but not the temperature.

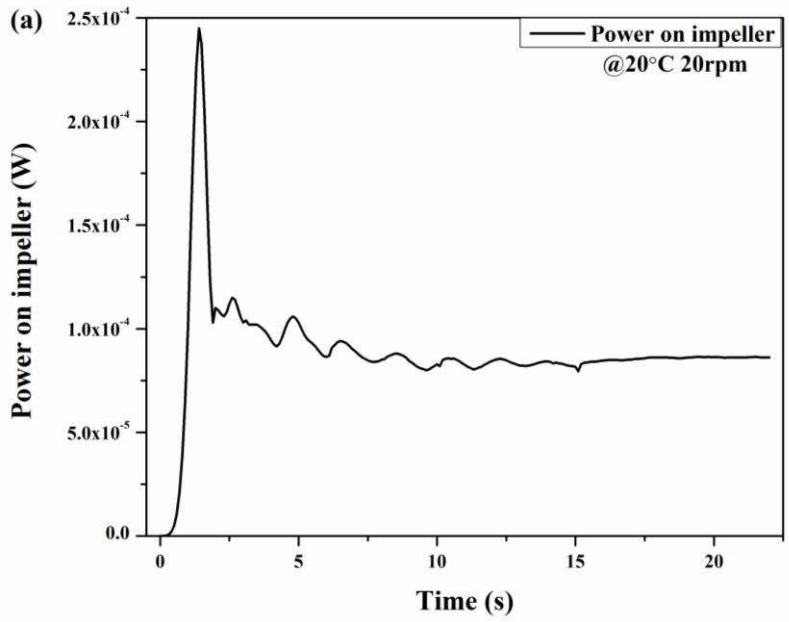

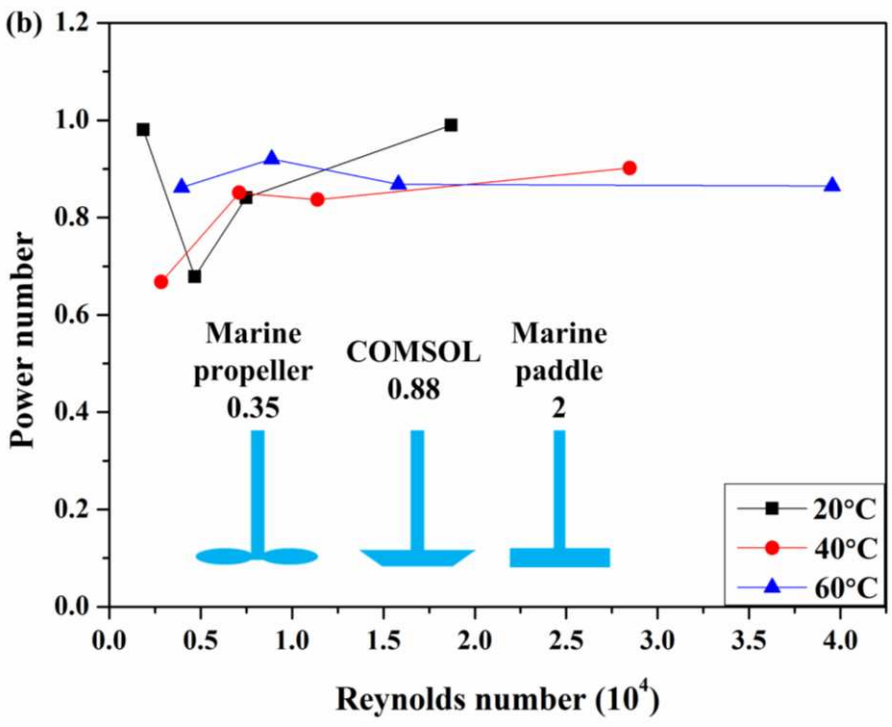

Figure 6. COMSOL simulation results of (a) power on impeller versus rotating time at 20 ºC 20 rpm and (b) power number versus Reynolds number. Embedded pictures in (b) are Marine propeller (power number 0.35) (Paul et al., 2004), impeller in the present work (average calculating power number 0.88) and Marine paddle (power number 2) (Paul et al., 2004) from left to right.

Table 3. Turbulent energy dissipation rate in the dissolution testing system with 800 mL water. Water density is used as ρ_f since the fluid is much diluted solution.

Temperature (°C)	N (rpm)	P (W)	ρ_f (kg/m^3)	ε (W/kg)
20	100	0.010	998	0.012
	200	0.077		0.097
	300	0.261		0.327
40	100	0.010	992	0.012
	200	0.077		0.097
	300	0.260		0.327
60	100	0.010	983	0.012
	200	0.076		0.097
	300	0.257		0.327

4.3. Model validation

Agitation generates shear flow around particles, and this shear flow accelerates the transport of solute to the bulk of solvent. In the present work, such an effect has been implemented into Sherwood number in Equation (10) as energy dissipation rate ε. The average energy dissipation rate from COMSOL simulation is employed in Equation (10) and (11) to predict particle dissolution behavior concerning particle size distribution in a bulk population of 0.15 g particles. To start with, modelling results are compared with experimental results for non-porous Na_2CO_3 granules showing in Figure 7.

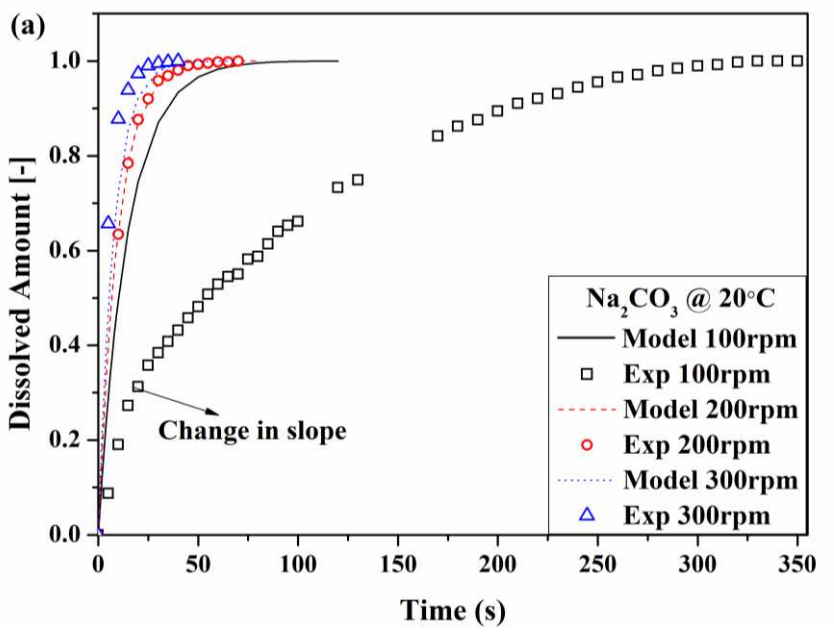

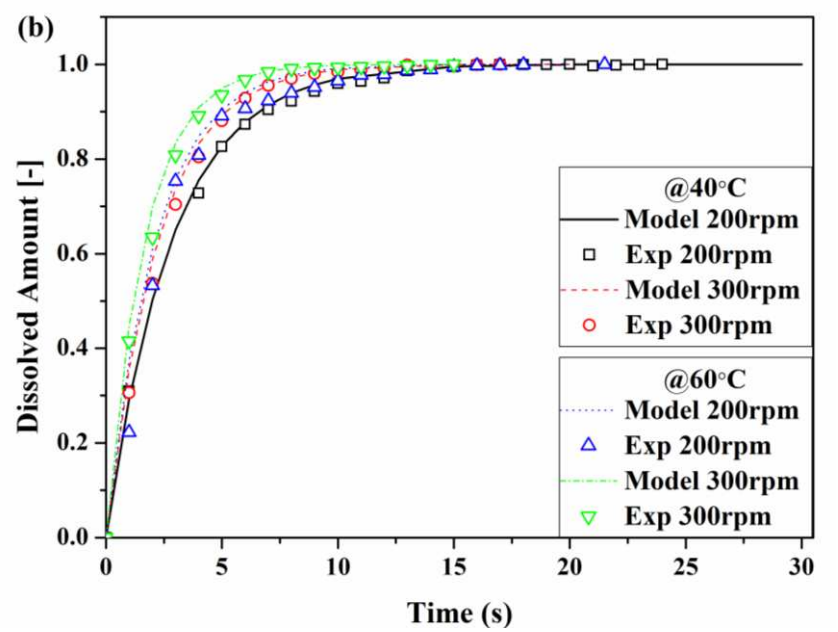

Figure 7. Experiment vs. modelling of Na_2CO_3 granule dissolving in the PTWS 610 mixing system at (a) 20 °C for 100, 200 and 300 rpm, and (b) 40 and 60 °C for 200 and 300 rpm.

Relatively good agreements of Na_2CO_3 granules dissolving at 200 and 300 rpm across the inspected three temperatures have been achieved between experiment and modelling. Dissolution results from modelling share the same trends throughtout the dissolution process. The total dissolution time from the modelling is longer than the experiment in most of the cases. Such a difference reduces as temperature and agitating speed increase, indicating that modelling results are more accurate for higher Reynolds number regime. However, the data for 100 rpm has been left out. Huge differences between experiment and modelling illustrate that the predicted dissolution profile is much faster than the experiment one. Detail information about energy dissipation rate ε within the vessel has been plotted in Figure 8 across the YZ-plane. Clearly in the images, from top to bottom, significantly higher ε has been dissipated for 300 rpm. Especially at the bottom, 300 rpm generates more than 30 times ε than 100 rpm at the same location, which indicates that particles in this area would endure much lower shear rate for 100

rpm. In experiment, due to the high density of Na_2CO_3 granules which limits the movement of particles during dissolution, particles tend to lump at the bottom of the vessel where local ε is much smaller than the average value used in modelling. Therefore, experiment dissolution rate is much lower than modelling one (see also the change of slope at time 20 s in Figure 7 (a)). From 100 rpm to 300 rpm, the differences between maximum ε value and minimum ε value in the vessel reduces, as a result, the average value of ε used in the model becomes more representative, hence much better agreements between modelling and experiment have been achieved. Such a result indicates that the accuracy of the developed model strongly relates with the Reynolds number in the dissolution system. In turbulent regime, the higher the Reynolds number, the higher the accuracy. Results also suggests that for those cases where the particles are not well mixed with the flow, either floating at the water surface or sinking around the bottom of the impeller region, using local values of the turbulent energy dissipation rate could potentially improve the accuracy of our model.

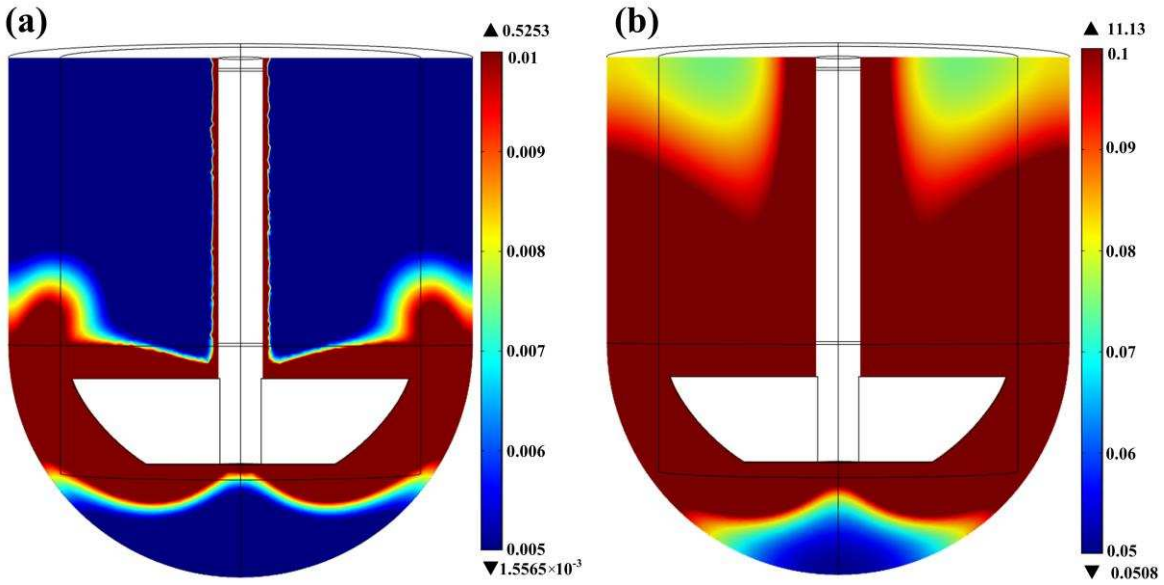

Figure 8. Turbulent dissipation rate from COMSOL simulation at 20 °C for rotating speed of (a) 100 rpm and (b) 300 rpm after equilibrium state has been achieved. Data were plotted on YZ plane. The scale in the images are the same as Figure 2.

Simulation results from Table 3 show that from 100 to 300 rpm, ε increases 27 times. Correspondingly, the total dissolution time decreases by 42 % in modelling and 89 % in experiment at 20 °C. Apart from agitation, temperature is another key factor for dissolution rate. In Figure 7, from 20 to 60 °C, the total dissolution time decreases by 75 % in modelling and 69 % in experiment at 200 rpm, then 79 % in modelling and 63 % in experimen at 300 rpm. The good agreements between experiment and modelling results show that the present framework can be used to predict non-porous single-ingredient particles dissolving in a well mixed system.

For the case of porous multi-ingredients particles PANDORA powders, the Nernst equation is not applicable due to the limited informaton about The cationic and anionic conductance of each ingredients in literature. As a result, comparison between experimental and modelling results at 20 °C 100 rpm was excuted first to obtain the diffusivity of this powder. Then Stokes-Einstein equation is used to calculate diffusivities at 40 and 60 °C.

Figure 9 (a) shows experiment vs. simulation results of PANDORA dissolution behavior for the two size cuts at 100, 200 and 300 rpm at 20 °C. With the diffusivity value obtained from 100 rpm, good agreement at 200 and 300 rpm has achieved. Similar to Na_2CO_3 granules, dissolution results from modelling share the same trends as experiment, and finish slightly faster than experiment in mode of the cases. However, different from Na_2CO_3 granule, PANDORA particles suspended very well in the vessel at 100 rpm due to its' porous strucutre (low density). As a result, no slope change of dissolution profile was observed. BET surface area of each size cuts, 0.332 m^2/g for 355-425 µm and 0.396 m^2/g for 425-600 µm, were not employed in the modelling. Instead, the surface area of a spherical particle was used which is the same as Na_2CO_3 granule. The SEM images in Figure 3 shows that PANDORA particles are irregular shaped aggolomerates. With a porosity of 0.41, it is understandable to use specific surface area in the

model. However, if specific surface area is used, the diffusivity of PANDORA at 20 °C 100 rpm will be 10^{-12} m^2/s, which is too small and normally exists between gas and solid (Hines and Maddox, 1984). This indicates that although particles have porous structures, the real contribution for these pores on dissolution is not reflected by the surface area exposing to water. An explanation could be that once contacting with water, the internal pores become saturated in a very short time due to the limited spaces (micron sized pores, seeing SEM images). According to Noyes-Whitney equation, the dissolution in these saturated internal pores stops until they expose to the outer flow. Therefore, the surface area of internal pores does not contribute to the dissolution of porous particles in the early stage. However, as particles continuously dissolving, dissolution in experiment is slightly faster than modelling which could be a indication that these internal pores expose to the outer flow and contribute to the overall dissolution.

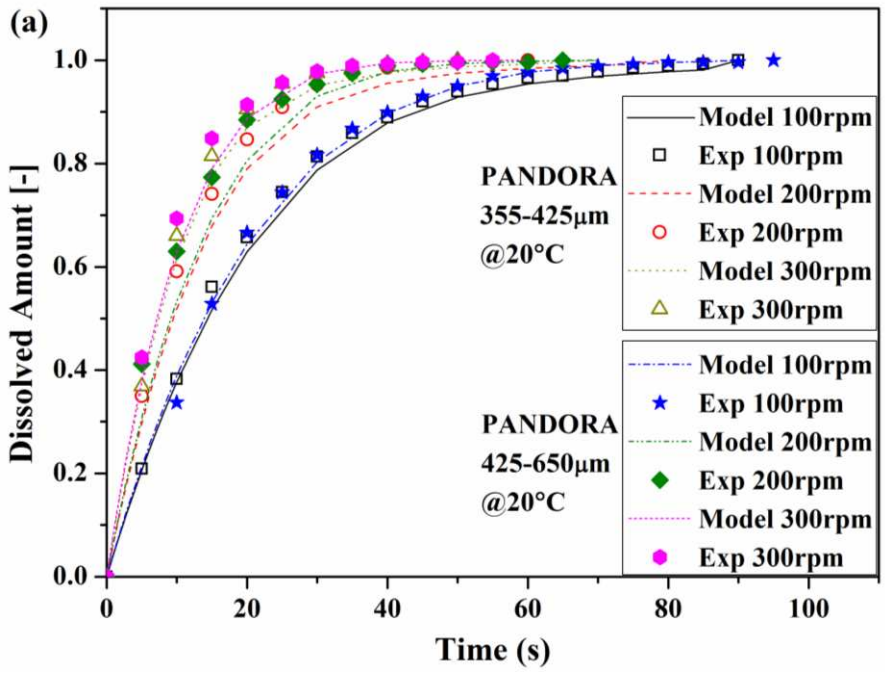

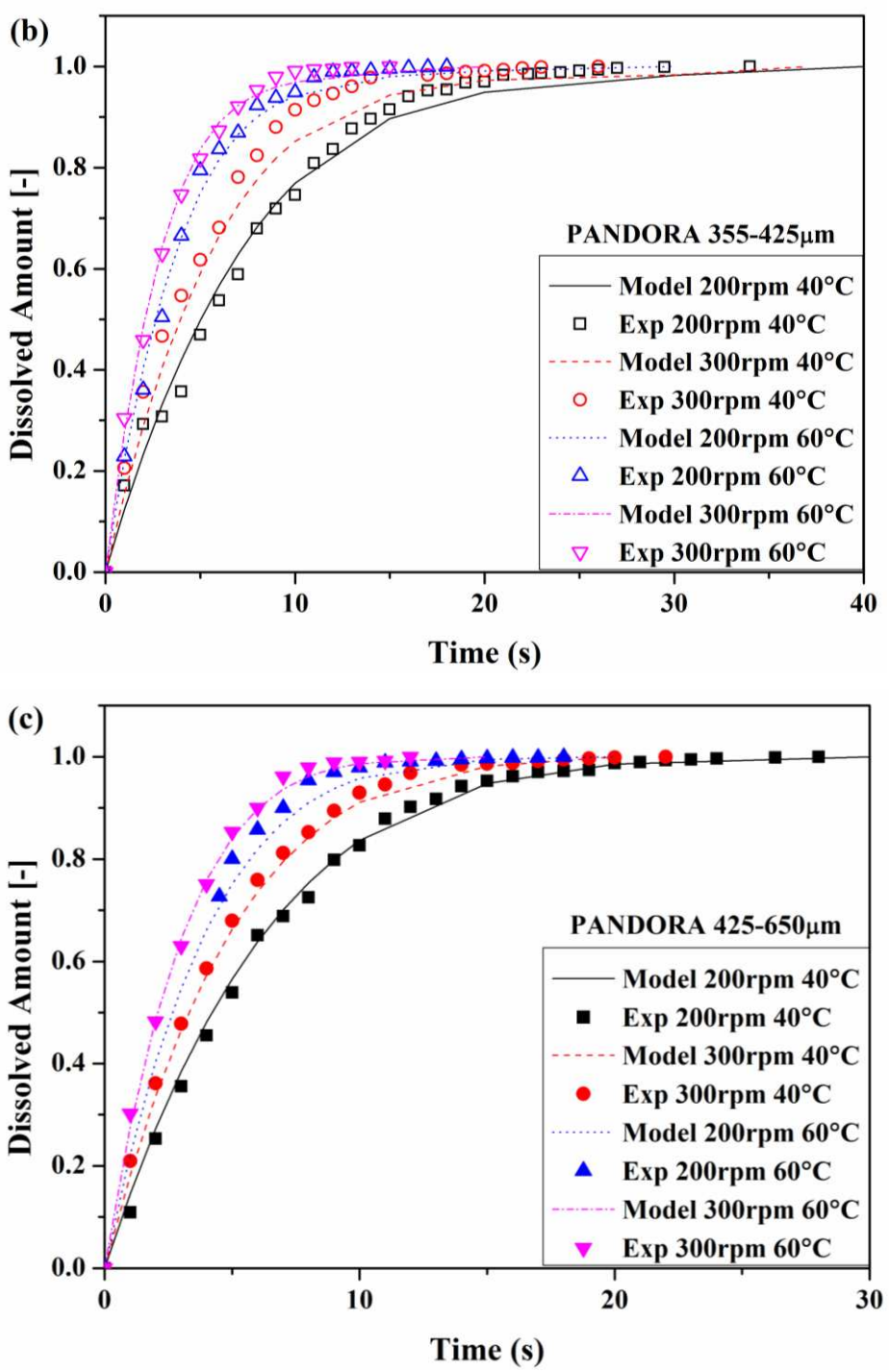

Figure 9. Experiment vs. modelling of PANDORA dissolving in the PTWS 610 mixing system at (a) 20 °C for 100, 200 and 300 rpm, (b) 40 and 60 °C for 200 and 300 rpm of size cut 355-425 µm and (c) 40 and 60 °C for 200 and 300 rpm of size cut 425-600 µm.

Figure 9 (b) and (c) show PANDORA dissolving at different temperature and agitating speed with size cuts 355-425 µm and 425-600 µm. At 40 and 60 °C, Stokes-Einstein equation was first

used to calculate the diffusivity based on the value at 20 °C. However, modelling results show much slower dissolution rate than experiment. Further modification of diffusivities at these two temperatures has been made according to experiment data at 100rpm, as shown in Table 4. After obtaining the correct diffusivity of PANDORA at investigated temperatures, predicting results from framework show very well agreement with experiment results at 200 and 300 rpm.

Table 4. Comparing of diffusivity from Stokes-Einstein estimation D_{SE} and experiment correcting value D_c (at 100 rpm) at different temperatures.

	PANDORA 355-425 µm		PANDORA 425-600 µm	
Temperature (°C)	D_{SE} ($\times 10^{-10}$ m^2/s)	D_c ($\times 10^{-10}$ m^2/s)	D_{SE} ($\times 10^{-10}$ m^2/s)	D_c ($\times 10^{-10}$ m^2/s)
20	-	1.00	-	1.20
40	1.07	2.00	1.28	2.50
60	1.14	2.80	1.36	2.80

Diffusivity of particles is one of the key parameters affecting predicting quality in our model. At different temperatures, Stokes-Einstein equation is a veryuseful approach to estimate particle diffusivity, especially for Na_2CO_3 granules in our first case. However, when particles become complex, for example PANDORA agglomerates which consist multi-ingredients, Stokes-Einstein equation is not suitable for estimating particle diffusivity. First reason is that the release order of each ingredients is unknown in the dissolution system. For single ingredients, the release rate can be consolted from literature. However, when these ingredients mix together inhomogeneously, the diffusivity of such an agglomerate can not be simply calculated by either one of the ingredients or a factor taking from each ingredients. Researchers have found that the lamellar phase of LAS coexists with a micellar solution (Richards et al., 2007), and this might

highly affect the diffusion of both LAS and the rest compositions in the PANDORA agglomerates. Other researches also point out that the first step of sodium silicate dissolving in water is to exchange the alkali ions with the hydrogen ions of the surround water, resulting in a protective layer of silanol group on the surface (Zoller and Sosis, 2008) which also might affect the diffusion of itself and the rest compositions. Second reason is that this equation is mainly for low Reynolds number flow regime. But more importantly, this equation is derived based on frictional force (also called drag force) exerting on sphere/spherical particles (Batchelor, 2000). Comparing to Na_2CO_3 granules, PANDORA agglomerates have irregular shapes with a large number of pores on the surface (seeing SEM images). With such a morphology, the failure of Stokes-Einstein equation is predictable. Apart from internal pores area and diffusivity, several other particle parameters in the model such as envelope density, solubility were estimated or measured as bulk particle properties. In reality, individual particle has slightly different properties across the size cut, which could be the reason affecting comparing quality between experiment and modelling. Nevertheless, the good agreements between experiment and modelling results indicate that once the accurate diffusivity of particles has been employed, the model is also capable of predicting the dissolution behaviour of porous multi-ingredients particles.

4. CONCLUSIONS

Combining CFD simulation and the Noyes-Whitney equation, particle dissolution behaviour has been directly linked with the input power of the mixing system in the present framework. With different dissolution conditions such as agitating speeds and temperatures, the validation results from experimet for both non-porous single ingredient particles and porous multi-ingredients particles have illustrated that the model is particularly capable of predicting bulk particles

dissolving in a flow regime where particles are well suspended in the mixing system. The direct link between the mixing system power and particle dissolution behaviour enables industry to minimize the amount of experimental work when extrapolating particle dissolution performance from bench scale measurements to any washing system/condition, which eventually could significantly shorter product design process. CFD simulation results of the detail information about turbulent energy dissipation rate within the mixing vessel indicate that for the case where particles are not well mixed, either floating on the surface or lumping at the bottom due to different envelope density of particles, local turbulent dissipation rate could be a further modification to make the model fully cabable of predicting all the dissolution conditions in the future.

ACKNOWLEDGMENT

The authors would like to give their acknowledgement to Proctor & Gamble Ltd., Newcastle Technical Centre for the research support.

REFERENCES

PTWS D610 Dual Drive Dissolution Tester.
Ansari, M.A., Stepanek, F., 2007. The Evolution of Microstructure in Three-Component Granulation and Its Effect on Dissolution. Particulate Science and Technology 26, 55-66.
Ansari, M.A., Stepanek, F., 2008. The effect of granule microstructure on dissolution rate. Powder Technology 181, 104-114.
Arnout, S., Verhaeghe, F., Blanpain, B., Wollants, P., 2008. Lattice Boltzmann model for diffusion-controlled indirect dissolution. Computers & Mathematics with Applications 55, 1377-1391.
Batchelor, G.K., 2000. An Introduction to Fluid Dynamics. Cambridge University Press.
Davidsohn, A., 1978. Spray drying and dry neutralization of powdered detergents. J Am Oil Chem Soc 55, 134-140.
Dressman, J.B., Fleisher, D., 1986. Mixing-Tank Model for Predicting Dissolution Rate Control of Oral Absorption. Journal of Pharmaceutical Sciences 75, 109-116.
Etacude, 2004-2008. Etacude.
Forny, L., Marabi, A., Palzer, S., 2011. Wetting, disintegration and dissolution of agglomerated water soluble powders. Powder Technology 206, 72-78.
Frenkel, J., 1946. Kinetic Theory of Liquids. Oxford: Clarendon Press.

Hemrajani, R.R., Tatterson, G.B., 2004. Mechanically Stirred Vessels, Handbook of Industrial Mixing. John Wiley & Sons, Inc., pp. 345-390.
Hines, A.L., Maddox, R.N., 1984. Mass Transfer: Fundamentals and Applications, 1 ed. Prentice Hall, New Jersey.
Jia, X., Williams, R.A., 2007. A Hybrid Mesoscale Modelling Approach to Dissolution of Granules and Tablets. Chemical Engineering Research and Design 85, 1027-1038.
Kang, Q., Zhang, D., Chen, S., He, X., 2002. Lattice Boltzmann simulation of chemical dissolution in porous media. Physical Review E 65, 036318.
Koganti, V., Carroll, F., Ferraina, R., Falk, R., Waghmare, Y., Berry, M., Liu, Y., Norris, K., Leasure, R., Gaudio, J., 2010. Application of Modeling to Scale-up Dissolution in Pharmaceutical Manufacturing. AAPS PharmSciTech 11, 1541-1548.
Nernst, W., 1888. Zur Kinetik der in Lösung befindlichen Körper. Erste Abhandlung. Theorie der Diffusion. Z. Phys. Chem. 2, 613-637.
Noyes, A.A., Whitney, W.R., 1897. THE RATE OF SOLUTION OF SOLID SUBSTANCES IN THEIR OWN SOLUTIONS. Journal of the American Chemical Society 19, 930-934.
Paul, E.L., Atiemo-Obeng, V.A., Kresta, S.M., 2004. Handbook of Industrial Mixing: Science and Practice. Wiley-IEEE.
Pereira Nunes, J.P., Blunt, M.J., Bijeljic, B., 2016. Pore-scale simulation of carbonate dissolution in micro-CT images. Journal of Geophysical Research: Solid Earth 121, 558-576.
Richards, C., Tiddy, G.J.T., Casey, S., 2007. Lateral Phase Separation Gives Multiple Lamellar Phases in a "Binary" Surfactant/Water System: The Phase Behavior of Sodium Alkyl Benzene Sulfonate/Water Mixtures. Langmuir 23, 467-474.
Robinson, R.A., Stokes, R.H., 2012. Electrolyte Solutions: Second Revised Edition. Dover Publications, Incorporated.
Schubert, H., 1987. Food particle technology. Part I: Properties of particles and particulate food systems. Journal of Food Engineering 6, 1-32.
Shah, Y.T., 1991. Design Parameters for Mechanically Agitated Reactors, in: James Wei, J.L.A.K.B.B., John, H.S. (Eds.), Advances in Chemical Engineering. Academic Press, pp. 1-206.
Smrčka, D., Dohnal, J., Štěpánek, F., Dissolution and disintegration kinetics of high-active pharmaceutical granules produced at laboratory and manufacturing scale. European Journal of Pharmaceutics and Biopharmaceutics.
Van Dalen, G., Nootenboom, P., Heussen, P.C.M., 2011. Correlative microscopy of detergent granules. Journal of Microscopy 241, 273-281.
Yuan, Q., Jia, X., Williams, R.A., 2013. Validation of a multi-component digital dissolution model for irregular particles. Powder Technology 240, 25-30.
Zoller, U., Sosis, P., 2008. Handbook of Detergents, Part F: Production. CRC Press.

NOMENCLATURE AND UNITS

A_0 initial surface area of particle, m^2

$A_{impeller}$ impeller surface area, m^2

1	A_t	exposing surface area of particle to solvent at time t, m^2
2	C_s	solubility of material (saturated concentration), kg/m^3
3	C_t	solute concentration at time t, kg/m^3
4	D	diffusivity, m^2/s
5	D_c	diffusivity from experiment correcting value, m^2/s
6	D_{SE}	diffusivity from Stokes-Einstein equation, m^2/s
7	F_c	Faraday constant, C/mol
8	$F_{impeller}$	force acting on each point of impeller surface, N
9	F_x, F_y	force components along x- and y-axis, N
10	K	dissolution rate constant, m/s
11	L	characteristic length, m
12	M_0	initial mass of particles, kg
13	M_t	remaining mass of particles at time t, kg
14	N	agitation speed, rpm
15	N_P	power number
16	$N_{particle}$	particles number
17	P	input power, W
18	R	ideal gas constant, J/(K*mol)
19	Sh	Sherwood number
20	T	temperature, K
21	V_f	volume of the solvent, m^3
22	Z_+	cation valence
23	Z_-	anion valence
24	$d_{impeller}$	diameter of impeller, m

1	$d_{p,0}$	initial particle diameter, m
2	$d_{p,t}$	particle diameter at dissolution time t, m
3	d_{tank}	diameter of stirring tank, m
4	k_B	Boltzmann's constant, J/K
5	r_p	radius of diffusing particle, m
6	t	time, s
7	(x,y,z)	spatial coordinates, m
8	Γ	torque on impeller, N*m
9	Ω	agitation speed, 1/s
10	ε	turbulent energy dissipation rate, W/kg
11	λ_+°	cationic conductance at infinite dilution
12	λ_-°	anionic conductance at infinite dilution
13	μ_f	solvent viscosity, kg/(m*s)
14	ρ_f	solvent density, kg/m^3
15	ρ_p	particle density, kg/m^3
16		